Title: Single-Nucleus Transcriptomics Reveals How Tissue Context Shapes the Circadian Transcriptome of the Arabidopsis Leaf

Alveena Zulfiqar[1†], Zachary A. Myers[1†], Ananda Menon[1] , and Kathleen Greenham[1,2]

[1]University of Minnesota, St. Paul, MN 55108, USA

† These authors contributed equally to this work.

[2]Author for correspondence: greenham@umn.edu

[2]Corresponding author:

University of Minnesota

St. Paul, MN 55108

Abstract

Background: Circadian regulation enables plants to coordinate cellular processes with daily environmental cycles, yet the dynamics and hierarchy of the clock across cells and tissue types remains poorly understood.

Results: We developed a 24 hour single nucleus RNA-sequencing (snRNA-seq) circadian time course of the mature *Arabidopsis thaliana* leaf to characterize circadian regulation across tissues. We captured ~30,000 nuclei across seven circadian time points, recovering all major leaf cell types. We identified over 7,400 genes with cluster-resolved circadian regulation, and used coexpression analysis to define five major temporal expression clades shared across all cell types. We leveraged these assignments to identify genes with cell type-specific temporal shifts in expression. Single cell gene regulatory networks (scGRNs) were generated for each cluster through GENIE3, identifying many shared and unique transcription factor (TF) target interactions across clusters. A close examination of CCA1 targets identified Photosystem II repair components in a subset of mesophyll cells and a large number of auxin-associated genes in only a handful of clusters despite robust expression in other clusters, suggestive of cell type-specific CCA1 target regulation.

Conclusions: Our results demonstrate the extent to which circadian transcriptional regulation is present in the mature Arabidopsis leaf, and highlight the immense complexity in cell type specific regulation. This dataset provides a high-resolution resource for dissecting circadian gene regulation at cellular resolution and advances our understanding of tissue-specific clock dynamics in plants.

Keywords: single-nuclei, transcriptome, gene regulatory network, circadian clock, Arabidopsis

Background

The Earth's rotation on its axis generates predictable fluctuations in the day-night cycle. Over time, organisms from unicellular to complex multicellular species, including humans, have evolved endogenous circadian oscillators [1]. These autonomous time-keeping mechanisms allow organisms to anticipate and adapt to these daily changes in light and temperature [1,2]. The circadian mediated alignment of cellular processes with external cues is central to survival and fitness [3]. Although clock genes vary across kingdoms, the fundamental principles of circadian regulation—such as transcriptional-translational feedback loops and entrainment by environmental cues known as zeitgebers—are remarkably conserved [4–8].

In plants, the circadian clock is integral to coordinating physiological processes with daily environmental changes, ensuring optimal growth, metabolism and development [9–11]. The plant circadian system consists of transcriptional regulators that function through transcriptional-translational feedback loops to generate rhythmic gene expression patterns with a roughly 24-hour period [12,13]. Dawn expressed *CIRCADIAN CLOCK ASSOCIATED 1* (*CCA1*) and *LATE ELONGATED HYPOCOTYL* (*LHY*) MYB transcription factors are followed by the sequential expression of the transcriptional repressors *PSEUDO RESPONSE REGULATORS PRR9, PRR7* and *PRR5* and the evening-phased *TIMING OF CAB EXPRESSION 1 (TOC1)/PRR1* [14–19]. Additional repressors include the Evening Complex (EC) consisting of *LUX ARRHYTHMO (LUX)-EARLY FLOWERING 3 (ELF3)* and ELF4 that contribute to circadian clock function and coordinating growth and development [20]. *NIGHT LIGHT-INDUCIBLE AND CLOCK-REGULATED1 (LNK1)*, and *LNK2* act as co-activators of *REVEILLE4* (*RVE4*) and *RVE8* to positively regulate *PRR5, TOC1* and the EC [19,21–23]. *LIGHT-REGULATED WD1* (*LWD1*) and

LWD2 are additional co-activators that along with *TEOSINTE BRANCHED 1-CYCLOIDEA-PCF20* (*TCP20* and *TCP22*) positively regulate *CCA1*, *PRR9,* and *PRR7 [24,25]*.

Unlike the centralized circadian control observed in mammals, where the suprachiasmatic nucleus (SCN) acts as the master pacemaker [26], plants possess a decentralized network of circadian oscillators distributed across tissues and organs [27]. Across certain tissue types there is evidence to suggest a complex hierarchical organization of circadian oscillators in plants. The shoot apical meristem (SAM) appears to serve as a dominant clock [28] providing long distance signaling to the root clock [29]. However, detached roots can maintain rhythmicity [30] suggesting the SAM is not required for clock function. Local signaling provides additional synchronization as observed in the leaf where the vascular clock appears dominant over the mesophyll clock [31]. Tissue-specific circadian clocks have been shown to regulate distinct physiological processes supporting the importance of local coupling of oscillators within a cell type. For example, the vascular clock plays a pivotal role in controlling flowering time via regulation of *FLOWERING LOCUS T (FT)* expression in phloem companion cells [31–33], while epidermal clocks modulate temperature-dependent cell elongation [32]. Overexpression of *CCA1* in guard cells led to enhanced water use efficiency (WUE) in a promoter specific manner, whereas no effect was observed when expression of *TOC1* was perturbed [34]. This suggests that both the guard cell clock and signaling from non-guard cell clocks are required for full response.

Several studies have shown that different plant tissues maintain distinct circadian periods [27,31,35–39]. In Arabidopsis seedlings, the cotyledon and hypocotyl have been found to exhibit shorter periods than the root [27,36,38]. Guard cells exhibited longer periods compared to adjacent

mesophyll and epidermal cells [40], and vascular tissues maintained more robust circadian rhythms compared to mesophyll cells [31,36]. Similarly, the *CHALCONE SYNTHASE* (*CHS*) promoter principally expressed in epidermal tissue has a longer period when compared with the mesophyll expressed Chlorophyll a/b-binding protein gene (*CAB*) [41]. In addition to organ level variation in circadian behavior, there are tissue level differences that reveal altered coupling of circadian oscillators across cell types. Within individual tissues, circadian rhythms vary spatially; regions of high cell density, such as shoot and root meristems, tend to have more tightly coupled clocks whereas the leaf can maintain independent phases of circadian clock gene promoter oscillations [28,37,39]. Single cell imaging of a pCCA1::CCA1-YFP fusion protein and bioluminescence recording of a LUCIFERASE (LUC) reporter driven by the promoter for the clock component *GIGANTEA* (*GI::LUC)* at near cellular level have revealed tissue-specific differences, such as the shorter periods observed in root tips compared to other regions across the root [27,38]. These tissue specific variations in clock behavior highlight the complexity of intra-tissue clock partitioning and emphasize the need to understand the importance of these distinct oscillators.

Traditionally, the study of plant circadian rhythms has been limited to methods such as bulk RNA sequencing (RNA-seq), which masks tissue-specific nuances by averaging signals across heterogeneous cell populations. However, recent technological advances, including single-cell and single-nuclei RNA-seq, have enabled unprecedented resolution, providing an opportunity to unravel cell specific circadian regulation. A snRNA-seq circadian time course on 8-day old Arabidopsis seedlings revealed highly conserved rhythmic expression of the core clock genes across most cell types, yet their phase and amplitude was highly variable. Consistent with tissue

specific roles of the circadian clock, most circadian regulated genes were expressed in specific cell types. Cotyledons exhibited more pronounced intra tissue cycling gene similarity than the root, although phase differences were observed across subclusters suggesting altered clock characteristics even within a tissue type [42,43]. A comprehensive understanding of how these tissue-specific oscillators regulate distinct biological processes will facilitate more targeted approaches for improving plant productivity and resilience.

In this study, we captured the transcriptional profiles of over 30,000 nuclei across a 24 hour circadian time course to investigate circadian regulation in mature leaves of Arabidopsis with single-nuclei resolution. This high-resolution analysis revealed the existence of distinct circadian oscillators operating within specific cell types and enabled us to identify five predominant phase dependent expression clades present across all cell types. Through a single cell gene regulatory network analysis we resolved cluster specific and conserved regulatory connections across cell types. Our findings provide new insights into the complexity of tissue specific circadian clock regulation across the leaf.

Results

Construction and cell type identification of a circadian single nucleus time course in mature leaves of Arabidopsis

To capture circadian clock regulated genes across different cell types in the Arabidopsis leaf, we conducted a single nucleus RNA sequencing (snRNA-seq) time course experiment on 13 day old Arabidopsis plants. We entrained seedlings to a 12 hour photoperiod at 22°C for 11 days prior to transfer to constant light (LL) (Fig 1A). Pairs of samples were collected over 24 hours at four-hour

intervals starting at ZT48 (zeitgeber, hours after dawn), isolating above-ground tissue by cutting over the root:shoot junction. Fresh tissue was immediately used for nuclei isolation and 10X Genomics-based single nuclei capture. Initial assessment of these libraries through Cellranger [44] revealed promising nuclei capture rates ranging from ~2,000-4,000 for most libraries, and median genes detected metrics were similar to several previously reported single nucleus libraries, ranging from ~1,000-1,500 genes detected (Table S1) [43,45,46]. We observed higher than expected levels of background RNA (as defined by the fraction of reads assigned to cells in Cellranger), likely due to our sampling decision to minimize handling time by skipping both fluorescence activated nuclei sorting and density gradient purification, and note that of the initial 14 snRNA-seq libraries, one library did not pass QC (ZT24B), and one library had reduced nuclei capture rates (Table S1) (ZT04B).

Previous research identified that unguided integration of time course datasets can lead to phase-specific clustering, where genes with peak expression at a certain time of day influence clustering and obfuscate cell type specific signatures [43,47]. Core clock components, such as *CCA1*, are widely expressed across cell types [27], and we reasoned that our experimental design might introduce phase-specific biases not captured in single time point single cell experiments. We observed that a large portion of cluster specific cell type markers identified in previous experiments have been shown to be circadian regulated (Fig 1B), with a handful of cell types defined by a majority of genes previously observed to cycle [48,49]. We found that we could achieve cell type specific clustering by masking ~7,000 circadian regulated genes from integration anchoring, and subsequently using a large set of 15,000 variable genes as integration anchors (Fig 1C). To construct our circadian gene list, we combined the full set of cycling genes identified in

Romanowski et. al, and merged this list with genes identified as cycling in our own pseudo-bulk data (see methods). Our time course captured ~30,000 high quality nuclei, with predicted identities from all the major tissue types found in the Arabidopsis leaf. A majority of the nuclei captured were identified as actively photosynthetic or of mesophyll origin, with relatively smaller numbers of well described cell types, such as guard cells, phloem companion cells, and dividing cells (Fig 1D). This includes many cell types with a high proportion of circadian regulated marker genes, such as guard cells, which were often missing or unresolved when integrated without masking.

Tissue and cell type assignments were confirmed by examining expression of previously reported marker genes (Table S2), and further refined by Gene Ontology (GO) enrichment analyses and cluster-specific biomarker analysis (Fig 1E-H, Table S3). Cluster-specific expression of previously reported marker genes identified clusters 6, 9 and 14 as phloem companion cells, dividing cells, and guard cells, respectively (Fig 1E). Examining the most significantly enriched GO terms in each cluster highlighted tissue of origin very effectively for mesophyll, epidermal, and photosynthetic cells, with GO terms associated with water use, fatty acid biosynthesis, and light harvesting among the most enriched terms for each tissue (Fig 1F, Table S1). Finally, we used cluster-specific biomarkers to refine our tissue and cell type assignments in many clusters (Fig S1). Expression of *FAMA*, a bHLH transcription factor involved in stomatal development [50], was highly specific to cluster 14, with moderate expression only found in cluster 13 (Fig 1G). Expression of *NPCC6* (*NUCLEAR-ENRICHED PHLOEM COMPANION CELL GENE 6*) was previously reported to be highly specific to phloem companion cells [51], and was identified as a highly significant cluster 6 biomarker in our dataset (Fig 1H).

Cycling gene expression is widespread across all cell types of the mature Arabidopsis leaf

As an initial quality check, we examined pseudo-bulk expression profiles of a handful of circadian clock components and outputs over our single nucleus time course (Fig 2A). We saw robust oscillations coinciding with previously reported expression patterns in all of the examined components [48,52,53]. We next examined whether these expression patterns persisted within and across clusters for a suite of circadian clock components (Fig 2B). We observed similar expression patterns across most clusters for *CCA1* and *TOC1*, where we observed robust and similar cycling across a large number of clusters. In contrast, many clock components were only identified as cycling in a subset of clusters. In most cases, such as with *GI, LUX*, and *PRR5*, patterns were consistent across clusters in which they were called cycling; however, a handful of clock components were observed with shifted phase in one or more clusters. One striking example of this is *ELF3*, which has an earlier phase in guard cells (Fig 2B). In order to better characterize these expression patterns, we utilized JTKcycle [54] to identify cycling genes using both pseudo-bulk and cluster-resolved expression values. We identified 4,769 genes with cycling gene expression patterns in our pseudo-bulked dataset (Table S4). Our analysis revealed that ~68% (3264/4769) of our rhythmic genes from the pseudo-bulk data set overlaps with a previous bulk-RNAseq circadian regulated gene list [48].

Cluster-specific cycling genes were identified for all clusters other than Cluster 16, where tissue sampling variability likely drove non-uniform distribution of root hair cell type across the time course (Fig S2). The total number of genes identified with cluster-specific cycling patterns ranged from ~1,800 in Cluster 0, to ~300 in Cluster 8_1 (Fig 2D, Table S5). While we noted that the clusters with the fewest identified cycling genes were also relatively small clusters, our ability to

consistently capture robust rhythms for key clock TFs such as CCA1 and TOC1 is encouraging (Fig 2B). We observed 4,825 genes cycling within at least one cluster, and noted that more than half of all cycling genes were identified as cycling in only a single cluster (Fig 2E). Examination of the phase of cycling markers in each cluster identified that most clusters contain genes with peak expression across our time course; however, a handful of clusters have clear biases towards cycling genes at key time periods, including an apparent over-representation of morning-phased cycling genes in guard cells (Fig S3). Many core clock components were identified as cycling in many clusters, with *CCA1* and *TOC1* significantly cycling in 18 and 14 clusters across the dataset respectively, and note that the shifted expression observed in *ELF3* in guard cells met our threshold for significance (Fig 2B). Due to our decision to process nuclei from fresh tissue at every time point, a 48 h time course was not feasible. To limit the false-negatives associated with capturing a single cycle we included a biological replicate at every time point to help reduce this concern, and have adopted a stringent significance threshold for cycling status [55].

Our analysis revealed 7,417 rhythmic genes across clusters with 59% overlapping with previous bulk RNA-seq data [48]Fig S4, [48]. Furthermore, we observe a significant overlap of cycling genes between our data set and a recent 24 h and 48 h circadian snRNA-seq data set [43], with 41% of genes identified as cycling genes in the 24 h dataset and 63% overlapping with the 48 h dataset (Fig S4). The high overlap with the 48 h time course supports our inclusion of a second replicate and indicates that we have identified a significant number of genes that have been previously reported as circadian regulated at bulk and at the single cell level.

Coexpression network analysis identifies five major temporal expression patterns across all cell types

Due to the limitations inherent in calling phase from a single 24 hour cycle [54] we confirmed the cycling and phase using the weighted gene correlation network analysis (WGCNA) package in R [56]. The method has been previously applied for grouping cycling genes with similar phases into modules [57,58]. This resulted in clustering of genes on the basis of expression pattern into 26 modules. To remove genes with weak correlations with the module eigengene pattern, we filtered the modules by kME (Module Eigengene connectivity) value; only genes with kME ≥ 0.6 were retained. We next calculated correlation metrics for the modules identified by using the average zScore of each module for the time course. We then used the metrics to perform hierarchical clustering of the modules. Euclidean distance calculated from the correlation values, where shorter distance indicates strong relationship and more similarity between the modules, identified five major clades among all modules. Representative expression patterns for each clade was calculated by averaging the zScore of all the genes and resulted in five major gene expression patterns throughout the day: early morning genes (clade 3), morning genes (clade 2), mid day genes (clade 1), evening genes (clade 4) and late night genes (clade 5) (Fig 3A, Table S6). Additionally, we examined the distribution of the five clades across our clusters and each tissue type had representation of all five expression patterns (Fig 3B). Some tissue types were more enriched in certain expression patterns, for example C5 (Vasculature) and C14 (GC) clusters had a larger proportion of genes with morning expression pattern (clade 2).

To analyze the biological processes enriched for the clades identified, we performed Gene Ontology (GO) enrichment analysis (Table S3). The GO analysis identified some common and

unique enrichment terms among the clades; the early morning clade (clade 3) had genes involved in auxin response, tropism and regulation of stomatal closure. Similarly, we saw enrichment of genes for indole-containing compound catabolic/biosynthesis processes and cellular response to ABA enriched in the midday clade (clade 2). The GO terms related to preparation for photosynthetic machinery were enriched in the second half of the day indicating the plant's strategy to prepare for the energy harvesting processes of the next day (Fig 3A).

To examine whether genes cycling across clusters exhibited similar phase patterns we identified genes that were found in multiple clades. The majority of genes (5611) were exclusive to one clade only, whereas 1540, 114, and 1 gene were found in 2, 3, and 4 clades respectively. For the genes present in two clades, we find most shifts occurred between adjacent clades (Fig 3C; grey ribbons); however, a small fraction of genes exhibited more dramatic anti-phase changes (Fig 3C; yellow ribbons). Examining these genes at the cluster level reveals similar changes between clusters suggesting a common regulatory mechanism (Fig. 3D). Notably, we identified a handful of genes in our photosynthesizing cluster that showed phase shifts when compared to phloem companion cell (PCC) or guard cell (GC), resulting in their segregation into different clades (Fig 3D). As our analysis revealed that the same genes can have tissue specific expression patterns, we next aimed to construct tissue-specific gene regulatory networks to enhance our understanding of the unique regulatory mechanism at play in each tissue type.

Single cell gene regulatory networks uncover tissue-specific regulation of gene expression through CCA1 in photosynthesis- and auxin-associated targets

We next constructed circadian single cell gene regulatory networks (scGRNs) to better characterize the ways in which circadian genes are differentially regulated across tissues. We implemented the GENIE3 algorithm on individual clusters while simultaneously limiting our input dataset to genes which are cycling in that specific cluster. In parallel, we iteratively shuffled each cluster's data and ran GENIE3 to identify null distributions of each dataset. The weight value corresponding to the 95th percentile was used as a weight cutoff for the unshuffled connections, leaving ~156,000 TF-target connections spread across all clusters (Fig 4A, Table S7). Approximately 25% of the edges had TFs and targets assigned to the same WGCNA clade, while the remaining 75% were assigned to different WGCNA clades (Fig 4B). The enrichment for similar expression patterns within TF-target edges suggests we have captured more instances of transcriptional activation than repression, which would naturally fall into different clades.

GRN target sets in individual clusters were broadly enriched for photosynthetic and circadian GO terms (Fig 4C), reflective of the strong regulatory control the clock exerts on the timing of photosynthetic activity and other rhythmic processes [52,59–61]. Comparison of the GRNs between clusters identified generally larger target overlaps between clusters of similar cell types (Fig 4D), supporting that different cell types within a common tissue maintain some amount of shared network structure. Enrichment was also identified for a number of environmental responsive terms, including temperature and light responses. Given that both light and temperature are key zeitgebers in plant circadian entrainment [62], examining the specific interactions underlying these enrichments could provide new insights into how clock entrainment is maintained in diverse cell types.

Many TFs had targets identified across multiple clusters, including CCA1, which had predicted targets in 18 of the 19 analyzed clusters. We saw that CCA1-centered networks were also more similar within similar tissue types, with Jaccard index based hierarchical clustering highlighting the similarity within mesophyll clusters and vascular clusters (Fig 4E). This relationship was also seen in other clock components, such as LNK2, PRR7, and TOC1; however, clock components identified as cycling in fewer clusters, such as LNK3 or ELF3, tended to only share overlap in mesophyll associated clusters (Fig S5).

As an initial step when examining TF-resolved scGRNs, we investigated overlap of CCA1 and PRR7 edges with previously published ChIP-seq datasets, identifying many overlapping targets and highlighting a subset of interactions for evaluation (Fig 5A). Examination of shared targets of CCA1 between pairs of clusters revealed that the similarity between CCA1-centered networks was largely driven by which and how many photosynthesis-associated targets were identified (Fig 5B). A suite of 11 light-harvesting chlorophyll a/b-binding proteins (LHCB) with CCA1 edges spanned at least 3 clusters, whereas 7 of the 9 CCA1 edges found in only one or two clusters were associated with Photosystem II repair, with 6 of these 20 CCA1-target pairs (Fig 5B) supported by ChIP-seq binding [63]. The combined action of broad light harvesting influence and cell type specific PSII repair targets of CCA1 highlight the complex and layered regulation by the clock to fine-tune photosynthetic activity.

In addition to the similarity of photosynthesis-associated targets across clusters, we also noted that auxin responsive genes in CCA1-centered networks contained a high proportion of edges restricted to a single cluster (Fig 5C). More than 20% of all genes assigned to auxin-responsive GO

categories were identified in CCA1-centered networks in at least one cluster, with edges called between CCA1 and 64 unique targets. A majority of these CCA1-target pairs were identified in Photosynthetic clusters c0 and c1; however, 13 pairs were unique to clusters other than c0 or c1, and an additional 21 pairs were present in at least one non-Photosynthetic cluster. To further support these TF-target connections, we again leveraged previously published CCA1 ChIP-seq experiments [63], identifying a subset of 18 TF-target edges supported by bulk ChIP-seq binding (Fig 5C). Given the single cell nature of our dataset, we were curious if we could identify instances of cell type specific CCA1 activity. While many of these ChIP-validated edges were only found in Photosynthetic cells, more than half were also present in at least one other tissue or cell type. Because our initial GRN construction was constrained to only cycling genes in each specific cluster, we noted genes which were included in network construction in at least one other cluster (Fig S6), identifying a total of 10 CCA1 target genes that were included in GRN construction for more clusters than a CCA1 edge was identified in.

Examination of the PRR7-centered networks identified many edges associated with red light signaling and abscisic acid signaling (Fig 5D-E). Similar to the CCA1 photosynthesis network, we observed predicted regulation of light harvesting complex (LHC) components by PRR7 across many clusters (Fig 5D). A majority of these PRR7-LHC edges were supported by previously published ChIP-seq binding data [64], again highlighting the strong connection between the circadian clock and the daily timing of photosynthetic capacity. Among edges detected only in one or two clusters, we observed several well-described light signaling components, including targets implicated as PRR7 bound in the referenced ChIP-seq dataset, such as *ELONGATED HYPOCOTYL5 (HY5)* and *SUPPRESSOR OF PHYA-105 1 (SPA1)*. The ABA-associated PRR7

network, similar to the photosynthesis-associated CCA1 network, contained a large proportion of edges identified in only one cluster. Of note is an edge identified between PRR7 and *GIBBERELLIC ACID INSENSITIVE (GAI)* in the Epidermal cluster 2, where GA has well defined roles in regulating organ growth and physiology [65,66]. More than half of the multi-cluster edges were also identified as PRR7 bound promoters in the referenced ChIP-seq dataset, including robust, wide-spread regulation of a suite of expected clock components (Fig5 5E). These PRR7 links to *CCA1, LHY, RVE2, RVE8,* and *ELF3* support that the scGRNs constructed and analyzed in this work have captured biologically relevant interactions between circadian regulated TFs and their varied targets across cell types.

Discussion

Unlike animals, plants lack a central nervous system, leading to a long-standing effort to uncover the nature of intercellular communication of circadian clocks in plants. Prior studies have demonstrated that Arabidopsis tissues have autonomous clocks that can anticipate environmental inputs and regulate responses [35,36,38,67,68]. To understand the nuances of the cell specific role of the circadian oscillator we conducted a single-nucleus RNA-Sequencing (snRNA-seq) time course experiment and constructed tissue specific circadian GRNs. In this study we captured ~30,000 nuclei and were able to identify all major tissue types as have been previously identified in other single cell/nuclei expression studies of leaf tissue [49,69,70]. This provided us the opportunity to identify tissue specific circadian regulated gene expression. As reported in earlier investigations, around 30% of the Arabidopsis transcriptome is circadian regulated with time of day (TOD) dependent expression patterns [48,52,53,71]. Not surprisingly, many of the marker genes commonly used for cell type identification during cluster annotation [49,69,70] have been

shown to be circadian regulated [48]. The substantial proportion of marker genes with TOD dependent expression patterns affected our ability to integrate the time course data into cell type specific clusters (Fig 1B). To resolve the cell type identities of the clusters, we decided to mask rhythmic genes from integration anchors to identify and annotate clusters in our time series experiment.

Following cell type clustering, we resolved 16 cluster populations, identified by previously reported marker genes and validated by GO analysis (Fig D-F). The clusters were further grouped into six major tissue types (Fig 1D) i.e. Mesophyll (M), Epidermis (E), Dividing cells (D), Vasculature (V) and Root Hair (RH). Although in our sampling approach we aimed to enrich the above ground tissue, identification of RH cells despite their low numbers validates our annotation strategy and its ability to pull out even small populations of cells with distinct identity. Our pseudo-bulk analysis shows cycling of *CCA1*, *LHY*, *PRRs*, *RVEs*, *LNKs* and other clock genes (Fig. 2A) with peak expression at their expected time of the day based on previous bulk RNA-seq studies [72]. Our cycling analysis of the sn-clusters revealed that many of these core clock genes cycle in most of the clusters identified (Fig. 2B). For example, *CCA1* cycled in all but one cluster, *TOC1* and *LHY* cycled in the vast majority of clusters (Fig. 3D). Therefore, our data suggests that core clock components oscillate robustly in all tissue types and signifies the presence of a functional clock at the tissue level. However, we do observe some core clock transcription factors (TFs) like *PRR5* and *LUX* exhibiting cyclical expression in only subsets of clusters identified as photosynthesizing, mesophyll, and epidermal for both, and in vascular cluster for *LUX*.

To be confident in the set of genes defined as rhythmic in our clusters we used WGCNA [56] to group genes with similar temporal expression patterns. We generated 26 network modules which were further grouped into five clades. All five-clades had distinct expression patterns and captured major phases of circadian rhythmic expression pattern throughout the day. Clades 5 and 3 capture the phase of morning expressed genes, clade 2 and 1 consist of genes that have midday expression patterns and clade 4 with evening expressed genes. Both *CCA1* and *LHY* were found in clade 3 and 5, consistent with their known dawn/morning phase of expression [18,73]. Similarly, *PRR9* and *PRR7* in 2/3, *PRR5* in clade 2/1, and *TOC1* in clade 4/1. The PRRs are a five-member family of proteins and are expressed sequentially from morning to night with the following order *PRR9*, *PRR7*, *PRR5*, *PRR3* and *TOC1 [74]*.

The GO enrichment of our temporal clades further validates previously known circadian regulation of physiological processes. Early morning clades were enriched for auxin response coinciding with previous findings that auxin responses are clock gated and the amplitude of expression of auxin response genes decline from morning to dusk and then are upregulated from dusk to dawn [75,76]. Similarly, the clock plays an important role in regulating ABA and stomatal responses [77]. We found enrichment of these responses particularly in the late night clade (Fig 3A). We also identified enrichment of salicylic acid (SA) mediated signalling pathways in our morning clade in accordance with previous findings that SA peaks in the middle of night and prepares plants for the immune response at dawn when plants are highly vulnerable to pathogen infection [78–80].

In our analysis, we identified genes cycling across multiple clusters that were segregated into two or more clades, suggesting altered circadian regulation of the same gene across tissues. Our

approach to scGRN construction was to develop individual networks for each cluster using only cycling gene expression (Fig. 4A). This allowed us to temporarily mask the influence of cell type specific regulation during network construction, and then regain it through comparison of cluster-resolved networks. We observed that many of the edges for CCA1 and PRR7 overlapped with ChIP-seq predicted targets for each TF, supporting that we have captured biologically relevant interactions in our networks (Fig. 5A). Interestingly, when comparing genes that were regulated across multiple clusters to genes regulated only in a single cluster, we identified broad regulation by CCA1 on light harvesting components, compared to more limited regulation by CCA1 on photosystem II repair components. One possible explanation is that the distinct mesophyll clusters we have identified are being clustered at least in part by their photosynthetic status; however, GO enrichment on cluster biomarker sets identified a significant enrichment for PSII repair terms in only one of five mesophyll clusters (cluster 1, Table S1).

Direct links tying the circadian clock to steady state PSII repair cycles are largely missing; however, endogenous cycling of phosphorylation status of repair components has been documented, with the key phosphorylation status regulators *STATE TRANSITION8 (STT8), STT8 HOMOLOG7 (STN7),* and *psbO* all showing circadian expression patterns [71,81,82]. Additionally, clock gating of PSII repair components has been described in response to stress conditions, including gating of SIGMA FACTOR5 (SIG5), a key regulator of the psbDC operon that is involved in D protein cycling [83–85]. The nuclear encoded protease *DEGRADATION OF PERIPLASMIC PROTEINS8 (DEG8)* is also involved in D protein cycling, was identified as a CCA1 target through scGRN predictions, and is supported by previously published CCA1 ChIP-

seq binding. Further examination of the relationship between CCA1 and DEG8 could solidify a regulatory link between the clock and steady state PSII repair cycles.

Alongside a significant role in optimizing the timing of expression of photosynthetic genes, the circadian clock is also intimately linked with auxin, having been shown to gate the biosynthesis, transport, and sensitivity of auxin within the plant [76,86]. This relationship between the clock and auxin occurs across many cell types, but details of cell type-specific clock regulation of auxin signalling remains largely unknown. A recent study examined circadian gene expression in Arabidopsis seedlings at the single nucleus resolution, identifying a subset of six *SAUR* genes cycling exclusively in the shoot epidermis [43]. Our scGRN-based approach identified 64 auxin-associated CCA1 targets across all clusters, including a subset of 21 genes previously identified as potential CCA1 targets through bulk ChIP-seq. Many of these genes robustly cycle in multiple clusters, yet lack predicted CCA1 regulation outside of a single cluster, suggesting a cell type-specific regulatory function that has been missed in bulk analyses. One example matching these criteria is *SMALL AUXIN UPREGULATED 15* (*SAUR15*), a ChIP-seq validated CCA1 target that is predicted to be CCA1 regulated in Photosynthetic c1, but not in Vascular c5 or Phloem Companion Cells c6. Similarly, *FLAVODOXIN-LIKE QUINONE REDUCTASE 1* (*FQR1*) is a ChIP-seq validated CCA1 target, and edges between the two were predicted in Photosynthetic c0 and Mesophyll c4, but not in Vascular c5 or Guard Cell c14. These interactions capture potential CCA1 regulation of target genes in a cell type specific manner, and begin to describe the multifaceted ways in which the clock coordinates auxin signaling across the mature Arabidopsis leaf.

Conclusion

This study provides a comprehensive cell type resolved view of circadian gene regulation in mature Arabidopsis leaves. Through snRNA-seq profiling across a full 24-hour time course, we reveal widespread circadian regulation across all major tissue types, uncovering over 7,000 genes with rhythmic expression and demonstrating that core oscillator components are active and cycling in nearly all clusters. By integrating coexpression-based phase assignment and constructing cluster-specific gene regulatory networks, we identified both broadly shared and cell type–restricted transcriptional programs. In particular, we show that key clock regulators such as CCA1 exhibit distinct regulatory wiring across tissues, targeting photosynthesis- and auxin-associated genes in a cell type specific manner. Ultimately, our work highlights the importance of cell type context in shaping circadian outputs and lays a foundation for future efforts to manipulate temporal regulation in a tissue-targeted manner.

Material and Methods

Plant Growth and Sampling

Arabidopsis Col seeds were surface sterilized for four hours by vapor phase sterilization (Clough and Bent, 1998). Water was added to sterilized seeds so that they were imbibed. Seeds were plated on half strength MS agar with 1% sucrose, pH 5.7. Seeds were then stratified at 4°C for two days in complete darkness. Following stratification plates were placed in a chamber with 12L/12D photoperiod (light intensity 130 µmol s^{-1}) at 22°C. Seedlings were entrained by 12L/12D conditions for 11 days. On the 11th day, starting at subjective dawn, seedlings were grown in constant light for 48 hours before the start of the time course. Leaf samples of 180-250 seedlings were harvested

by cutting across the root-shoot junction in replicates for single-nuclei RNA-seq every 4 hours over a 24-hour period starting at the subjective dawn of the 13th day.

Nuclei Isolation

Leaf tissue was collected in a petri plate containing 5 ml of pre chilled NIB (10mM Tris-HCL-pH 7.4, 10 mM NaCl, 3 mM MgCl, 0.5mM Spermidine, 0.2 mM Spermine, 0.5% BSA with PI and 0.03 U/µl of RNAse inhibitor but without detergents). Leaf samples were chopped at 4°C for 3 min with a razor blade. Finely chopped leaf samples were then shifted to 50 ml falcon tubes, ~ 15 ml of NIB was added to make the final volume of sample 20 ml. Samples were incubated on a rotating platform for 5 min to facilitate release of cells. After the first incubation, samples were filtered via 70 µm and 40 µm cell strainers to remove leaf debris. Triton X-100 and NP-40 were added to final concentration of 0.05% and extracts were incubated on a rotating platform at 4°C for 10 min. The nuclei suspension was then centrifuged at 500 x g for 5 min at 4°C. The nuclei pellet was then resuspended in 5 ml of NIB without detergents and was again pelted at 500 x g for 5 min at 4°C. The pellet was resuspended in 750 µl of resuspension buffer. Nuclei suspension was then shifted to the Nuclei Isolation column and collection tube of the Chromium nuclei isolation kit (PN-10000494, 10X Genomics, Pleasanton CA). Samples were then centrifuged at 16000 x g for 40 seconds. Pelleted nuclei were finally resuspended in 500 µl of resuspension buffer. Nuclei were counted manually with a hemocytometer. The 32k nuclei were loaded onto the 10x Genomics Chip M, which was then processed with 10x Genomics Chromium X controller, and sequencing libraries were constructed following manufacturer's instructions (PN-1000268 number for the kit, 10X Genomics, Pleasanton CA). Total time from leaf harvest to loading was between 30-40 min.

Data Availability

All code used to process and analyze the reported data is available at https://github.com/GreenhamLab. Raw sequencing data and processed Seurat objects are available upon publication through SRA.

Data Analysis

Cell Ranger (v7.0.1) was used to generate gene by cell matrices from Demultiplexed FASTQ files by aligning with Arabidopsis TAIR10 genome. Downstream analyses were performed with Seurat (v5.1.0). Cells with low numbers of UMIs, plastid contamination, or potential doublets identified through scDblFinder version 1.2 [87], were removed using Median Absolute Deviation filtering.

After initial filtering and discarding low quality cells, the data was normalized by using the "LogNormalize" global scaling method. Following normalization, highly variable features were computed for cells of the dataset. Then we used Principal Component Analysis for linear transformation and linear dimensionality reduction. After identifying the significant PCs, we implemented a graph-based clustering algorithm. Cells were embedded in a K-nearest neighbor graph structure, with cells with similar expression patterns having edges drawn to connect them followed by partitioning into communities. To cluster the cells, Louvain algorithm is applied based on 30 top PCs.

Pseudo bulk samples were generated by aggregating the raw counts from each cell of samples at sample and cluster level to identify oscillating gene expression. We used DeSeq2 to generate the normalized count matrix. For detecting expression of genes that oscillate throughout the time course we used METACYCLE [88]. METACYCLE uses three different cycling detection

algorithms i.e. meta2d: integrated ARSE, JTK-CYCLE and LS. We utilized JTK-CYCLE output to identify genes whose expression oscillates by setting cut-off Adj p-value < 0.05. Number of oscillating genes that were either specific to a cluster or shared between different clusters were illustrated by UpSet plots using the package UpSetR implemented under the *R* environment [89]. JTK-CYCLE accurately measures the phase, period, and amplitude. We used phase information for each gene and calculated phase difference of genes that were shared between different clusters to identify genes that were oscillating with different phases in between different clusters. To validate the phase difference observed, we used the WGCNA package to analyze genes for all clutters together with cluster identifiers. Gene with similar expression patterns were clustered together in the same module, whereas those with different phases segregated out into different modules.

scGRN Construction

Single cell GRNs were built with SCENIC implementation of GENIE3 [90,91] by subsetting the single nucleus dataset into individual clusters and proceeding only with data from cycling genes. Several steps of the scGRN construction were adapted from the scPlant R package [92]. To identify an appropriate weight threshold for each network, we shuffled our gene expression matrix and identified the weight value corresponding to the 95th percentile for each cluster individually. This weight was used as a cutoff for our unshuffled networks. Networks were visualized and annotated in Cytoscape [93].

Acknowledgements

This work was supported by the resources and staff at the University of Minnesota Genomics Center who performed all sequencing on this project, and by the resources and staff at the University of Minnesota University Imaging Centers (UIC, SCR_020997) who assisted with sample preparation assessment. We wish to thank Danielle Shoenecker for assistance with plant growth and care, and Rui Kuang for feedback on data processing approaches.

Funding

This project was supported by funding from NIH NIGMS 5R35GM14837-03.

Figure Legends

Figure 1. Major cell and tissue types can be resolved in the mature Arabidopsis leaf over a circadian time course. (**A**) Growth and sampling schematic used to generate the snRNA-seq dataset. (**B**) The proportion of cell type marker genes identified that are under circadian regulation. (**C**) UMAP projection of the fully integrated, cycling-masked snRNA-seq dataset (top), and the number of nuclei identified in each cluster (bottom). (**D**) UMAP projection, highlighting broader tissue types alongside more specialized cell types (top), and the violin plots describing the distribution of genes expressed in each group (bottom). (**E**) Scaled expression heatmap of a suite of previously identified cell type specific genes across the snRNA-seq time course. (**F**) Gene Ontology biological process enrichments of cluster biomarkers support expected cell type specific activities. (**G-H**) Expression feature plots for *FAMA* (FMA, AT3G24140) and *NUCLEAR-ENRICHED PHLOEM COMPANION CELL GENE 6* (NPCC6, AT5G02600), significant cluster biomarkers for guard cells (cluster 14) and phloem companion cells (cluster 6) respectively. D,

Dividing; E, Epidermis; GC, Guard Cell; M, Mesophyll; M/E, Mesophyll/Epidermis; P, Photosynthesizing; PCC, Phloem Companion Cell; PP, Phloem Parenchyma; R, Root; RH, Root Hair; T/E, Trichome/Epidermis; V, Vascular; X, Xylem.

Figure 2. Single nucleus RNA-sequencing captures circadian gene expression across diverse cell types of the mature Arabidopsis leaf. (**A**) Pseudo-bulk expression levels of key clock components and outputs over a circadian day. (**B**) Cluster-resolved expression of *CCA1* (top left), *TOC1* (bottom left), , and *LUX* (top center), *GI* (bottom center), *ELF3* (top right), and *PRR5* (bottom right) over a circadian day. Asterisks indicate a significant cycling call in the associated cluster. (**C**) Number of cycling genes identified through CycleJTK in each cluster. (**D**) Distribution of genes based on how many clusters in which they were called cycling. The presence of key clock TFs are indicated above the relevant groups.

Figure 3. Identification of temporal expression patterns across cell types through WGCNA and characterization of cell type specific phase changes in circadian expression. **(A)** Hierarchical clustering of WGCNA modules identified five major temporal clades. The average zScore for genes in each clade was plotted to get the representative expression pattern across clades. The ribbon represents the standard deviation. A selection of significantly GO enriched terms is included below each clade. (**B)** Proportional distribution of clades across clusters. **(C)** The circos plot shows the genes with a change in phase across two clusters resulting in placement in two different clades. The width of the ribbon signifies the number of genes with a phase change. Grey ribbon shows shifts to the adjacent clades, while the yellow ribbon represents shifts across clades (**D)** Expression pattern differences of sets of genes found cycling across

different tissue types. The average zScore of the genes within each cluster is shown to highlight the phase difference. Ribbons represent standard deviation.

Figure 4. Construction and evaluation of circadian, cluster-resolved single cell gene regulatory networks (scGRNs). (**A**) Schematic detailing the steps used to generate and filter scGRNs. (**B**) Number of scGRN edges where the TF and target are assigned to the same or different WGCNA clades. (**C**) Gene ontology biological process enrichment, showing the top 5 most enriched categories for each cluster. Photo, Photosynthetic; Meso, Mesophyll; Epi, Epidermis; GC, Guard Cell; Div, Dividing; Vasc, Vascular; PCC, Phloem Companion Cell; PP, Phloem Parenchyma. (**D**) Jaccard Index similarity matrix between pairs of clusters, using all significant edges identified. (**E**) Jaccard Index similarity matrix between pairs of clusters, restricted to significant CCA1-centered networks.

Figure 5. Examination of TF-resolved scGRNs for CCA1 and PRR7. (**A**) Overlap between scGRN edges identified in this study, and targets of CCA1 (left) or PRR7 (right) in previously published ChIP-seq experiments. (**B-E**) Node color indicates how many clusters an edge was identified in. Red edges and borders indicate support for an interaction through previously published ChIP-seq data. (**B**) CCA1-centered network built from all significant edges associated with the Photosynthesis GO:0015979 category. (**C**) CCA1-centered network built from all significant edges associated with the Response to Auxin GO:0009733 category. (**D**) PRR7-centered network built from all significant edges associated with the Response to Red Light GO:0010114 category. (**E**) PRR7-centered network built from all significant edges associated with the Response to Abscisic Acid GO:0009737 category.

Figure S1. Top cluster biomarkers for all identified clusters. Expression feature plots (top) and cluster-based expression violin plots (bottom) for two genes with the highest average expression fold change between clusters.

Figure S2. Distribution of root hair cells inadvertently captured across each library. These cell types were not specifically targeted during collection and are expected in low abundance.

Figure S3. Distribution of peak expression for cycling genes in each cluster. LAG represents peak expression or phase across the circadian day, as determined through CycleJTK.

Figure S4. Overlap in cycling gene identification across studies. (A) Overlap of pseudobulk-resolved cycling genes in our study with genes identified as cycling in Romanowski et al. (B) Overlap of cluster-resolved cycling genes in our study with genes identified as cycling in both the 24- and 48-hour Qin et al datasets.

Figure S5. Jaccard similarity indices for several circadian clock components. Similarity indices were calculated between all pairs of clusters for *LNK2, PRR7, TOC1, LNK3*, and *ELF3*, with darker blue indicating more similar scGRNs.

Figure S6. Cluster-resolved expression for genes identified as *CCA1* targets through scGRN prediction and supported by previously published ChIP-seq binding data. Genes are displayed as rows, with time points as columns. Red shading indicates clusters where a gene was

cycling and predicted to be *CCA1*-regulated, while blue shading indicates clusters where a gene was cycling but not predicted to be *CCA1*-regulated.

References

1. Saini R, Jaskolski M, Davis SJ. Circadian oscillator proteins across the kingdoms of life: structural aspects. BMC Biol. 2019;17:13.

2. Micklem CN, Locke JCW. Cut the noise or couple up: Coordinating circadian and synthetic clocks. iScience. 2021;24:103051.

3. Ouyang Y, Andersson CR, Kondo T, Golden SS, Johnson CH. Resonating circadian clocks enhance fitness in cyanobacteria. Proc Natl Acad Sci U S A. 1998;95:8660–4.

4. Achermann P, Kunz H. Modeling circadian rhythm generation in the suprachiasmatic nucleus with locally coupled self-sustained oscillators: phase shifts and phase response curves. J Biol Rhythms. 1999;14:460–8.

5. Adams S, Manfield I, Stockley P, Carré IA. Revised morning loops of the Arabidopsis circadian clock based on analyses of direct regulatory interactions. PLoS One. 2015;10:e0143943.

6. Akashi M, Takumi T. The orphan nuclear receptor RORα regulates circadian transcription mammalian core-clock Bmal1. Nature structural & molecular biology. 2005;12:441–8.

7. Glossop NRJ, Hardin PE. Central and peripheral circadian oscillator mechanisms in flies and mammals. J Cell Sci. 2002;115:3369–77.

8. Hastings MH, Reddy AB, Maywood ES. A clockwork web: circadian timing in brain and periphery, in health and disease. Nat Rev Neurosci. 2003;4:649–61.

9. Greenham K, McClung CR. Integrating circadian dynamics with physiological processes in plants. Nat Rev Genet. 2015;16:598–610.

10. Dodd AN, Salathia N, Hall A, Kévei E, Tóth R, Nagy F, et al. Plant circadian clocks increase photosynthesis, growth, survival, and competitive advantage. Science. 2005;309:630–3.

11. Graf A, Schlereth A, Stitt M, Smith AM. Circadian control of carbohydrate availability for growth in Arabidopsis plants at night. Proc Natl Acad Sci U S A. 2010;107:9458–63.

12. Pokhilko A, Fernández AP, Edwards KD, Southern MM, Halliday KJ, Millar AJ. The clock gene circuit in Arabidopsis includes a repressilator with additional feedback loops. Mol Syst Biol. 2012;8:574.

13. Nohales MA, Kay SA. Molecular mechanisms at the core of the plant circadian oscillator. Nat Struct Mol Biol. 2016;23:1061–9.

14. Strayer C, Oyama T, Schultz TF, Raman R, Somers DE, Más P, et al. Cloning of the Arabidopsis clock gene TOC1, an autoregulatory response regulator homolog. Science. 2000;289:768–71.

15. Nakamichi N, Kiba T, Henriques R, Mizuno T, Chua N-H, Sakakibara H. PSEUDO-RESPONSE REGULATORS 9, 7, and 5 are transcriptional repressors in the Arabidopsis circadian clock. Plant Cell. 2010;22:594–605.

16. Alabadí D, Oyama T, Yanovsky MJ, Harmon FG, Más P, Kay SA. Reciprocal regulation between TOC1 and LHY/CCA1 within the Arabidopsis circadian clock. Science. 2001;293:880–3.

17. Schaffer R, Ramsay N, Samach A, Corden S, Putterill J, Carré IA, et al. The late elongated hypocotyl mutation of Arabidopsis disrupts circadian rhythms and the photoperiodic control of flowering. Cell. 1998;93:1219–29.

18. Wang ZY, Tobin EM. Constitutive expression of the CIRCADIAN CLOCK ASSOCIATED 1 (CCA1) gene disrupts circadian rhythms and suppresses its own expression. Cell. 1998;93:1207–17.

19. Xie Q, Wang P, Liu X, Yuan L, Wang L, Zhang C, et al. LNK1 and LNK2 are transcriptional coactivators in the Arabidopsis circadian oscillator. Plant Cell. 2014;26:2843–57.

20. Nusinow DA, Helfer A, Hamilton EE, King JJ, Imaizumi T, Schultz TF, et al. The ELF4-ELF3-LUX complex links the circadian clock to diurnal control of hypocotyl growth. Nature. 2011;475:398–402.

21. Rugnone ML, Faigón Soverna A, Sanchez SE, Schlaen RG, Hernando CE, Seymour DK, et al. LNK genes integrate light and clock signaling networks at the core of the Arabidopsis oscillator. Proc Natl Acad Sci U S A. 2013;110:12120–5.

22. Rawat R, Takahashi N, Hsu PY, Jones MA, Schwartz J, Salemi MR, et al. REVEILLE8 and PSEUDO-REPONSE REGULATOR5 form a negative feedback loop within the Arabidopsis circadian clock. PLoS Genet. 2011;7:e1001350.

23. Farinas B, Mas P. Functional implication of the MYB transcription factor RVE8/LCL5 in the circadian control of histone acetylation: Role of RVE8/LCL5 in the circadian clock. Plant J. 2011;66:318–29.

24. Wang Y, Wu J-F, Nakamichi N, Sakakibara H, Nam H-G, Wu S-H. LIGHT-REGULATED WD1 and PSEUDO-RESPONSE REGULATOR9 form a positive feedback regulatory loop in the Arabidopsis circadian clock. Plant Cell. 2011;23:486–98.

25. Wu J-F, Tsai H-L, Joanito I, Wu Y-C, Chang C-W, Li Y-H, et al. LWD-TCP complex activates the morning gene CCA1 in Arabidopsis. Nat Commun. 2016;7:13181.

26. Ma M, Elizabeth H. Neuroanatomy, nucleus suprachiasmatic. 2019.

27. Gould PD, Domijan M, Greenwood M, Tokuda IT, Rees H, Kozma-Bognar L, et al. Coordination of robust single cell rhythms in the Arabidopsis circadian clock via spatial waves of gene expression. Elife [Internet]. 2018;7. Available from: http://dx.doi.org/10.7554/elife.31700

28. Takahashi N, Hirata Y, Aihara K, Mas P. A hierarchical multi-oscillator network orchestrates the Arabidopsis circadian system. Cell. 2015;163:148–59.

29. Ikeda H, Uchikawa T, Kondo Y, Takahashi N, Shishikui T, Watahiki MK, et al. Circadian clock controls root hair elongation through long-distance communication. Plant Cell Physiol. 2023;64:1289–300.

30. Li Y, Wang L, Yuan L, Song Y, Sun J, Jia Q, et al. Molecular investigation of organ-autonomous expression of Arabidopsis circadian oscillators: Organ-autonomous expression of clock oscillators. Plant Cell Environ. 2020;43:1501–12.

31. Endo M, Shimizu H, Nohales MA, Araki T, Kay SA. Tissue-specific clocks in Arabidopsis show asymmetric coupling. Nature. 2014;515:419–22.

32. Shimizu H, Katayama K, Koto T, Torii K, Araki T, Endo M. Decentralized circadian clocks process thermal and photoperiodic cues in specific tissues. Nat Plants. 2015;1:15163.

33. Voß U, Wilson MH, Kenobi K, Gould PD, Robertson FC, Peer WA, et al. The circadian clock rephases during lateral root organ initiation in Arabidopsis thaliana. Nat Commun. 2015;6:7641.

34. Simon NML, Graham CA, Comben NE, Hetherington AM, Dodd AN. The circadian clock influences the long-term water use efficiency of Arabidopsis. Plant Physiol. 2020;183:317–30.

35. Thain SC, Hall A, Millar AJ. Functional independence of circadian clocks that regulate plant gene expression. Curr Biol. 2000;10:951–6.

36. James AB, Monreal JA, Nimmo GA, Kelly CL, Herzyk P, Jenkins GI, et al. The circadian clock in Arabidopsis roots is a simplified slave version of the clock in shoots. Science. 2008;322:1832–5.

37. Wenden B, Toner DLK, Hodge SK, Grima R, Millar AJ. Spontaneous spatiotemporal waves of gene expression from biological clocks in the leaf. Proc Natl Acad Sci U S A. 2012;109:6757–62.

38. Greenwood M, Domijan M, Gould PD, Hall AJW, Locke JCW. Coordinated circadian timing through the integration of local inputs in Arabidopsis thaliana. PLoS Biol. 2019;17:e3000407.

39. Fukuda H, Nakamichi N, Hisatsune M, Murase H, Mizuno T. Synchronization of plant circadian oscillators with a phase delay effect of the vein network. Phys Rev Lett. 2007;99:098102.

40. Yakir E, Hassidim M, Melamed-Book N, Hilman D, Kron I, Green RM. Cell autonomous and cell-type specific circadian rhythms in Arabidopsis. Plant J. 2011;68:520–31.

41. Thain SC, Murtas G, Lynn JR, McGrath RB, Millar AJ. The circadian clock that controls gene expression in Arabidopsis is tissue specific. Plant Physiol. 2002;130:102–10.

42. Apelt F, Mavrothalassiti E, Gupta S, Machin F, Olas JJ, Annunziata MG, et al. Shoot and root single cell sequencing reveals tissue- and daytime-specific transcriptome profiles. Plant Physiol. 2022;188:861–78.

43. Qin Y, Liu Z, Gao S, Martínez-Vasallo C, Long Y, Zhu X, et al. 48-hour and 24-hour time-lapse single-nucleus transcriptomics reveal cell-type specific circadian rhythms in Arabidopsis. Nat Commun. 2025;16:4171.

44. Zheng GXY, Terry JM, Belgrader P, Ryvkin P, Bent ZW, Wilson R, et al. Massively parallel digital transcriptional profiling of single cells. Nat Commun. 2017;8:14049.

45. Wang K, Zhao C, Xiang S, Duan K, Chen X, Guo X, et al. An optimized FACS-free single-nucleus RNA sequencing (snRNA-seq) method for plant science research. Plant Sci. 2023;326:111535.

46. Guo X, Wang Y, Zhao C, Tan C, Yan W, Xiang S, et al. An Arabidopsis single-nucleus atlas decodes leaf senescence and nutrient allocation. Cell. 2025;188:2856–71.e16.

47. Wen S ’ang, Ma D, Zhao M, Xie L, Wu Q, Gou L, et al. Spatiotemporal single-cell analysis of gene expression in the mouse suprachiasmatic nucleus. Nat Neurosci. 2020;23:456–67.

48. Romanowski A, Schlaen RG, Perez-Santangelo S, Mancini E, Yanovsky MJ. Global transcriptome analysis reveals circadian control of splicing events in Arabidopsis thaliana. Plant J. 2020;103:889–902.

49. Lee TA, Nobori T, Illouz-Eliaz N, Xu J, Jow B, Nery JR, et al. A single-nucleus atlas of seed-to-seed development in Arabidopsis [Internet]. bioRxiv. 2023. p. 2023.03.23.533992. Available from: https://www.biorxiv.org/content/10.1101/2023.03.23.533992v1

50. Bergmann DC, Lukowitz W, Somerville CR. Stomatal development and pattern controlled by a MAPKK kinase. Science. 2004;304:1494–7.

51. Zhang C, Barthelson RA, Lambert GM, Galbraith DW. Global characterization of cell-specific gene expression through fluorescence-activated sorting of nuclei. Plant Physiol. 2008;147:30–40.

52. Harmer SL, Hogenesch JB, Straume M, Chang HS, Han B, Zhu T, et al. Orchestrated transcription of key pathways in Arabidopsis by the circadian clock. Science. 2000;290:2110–3.

53. Covington MF, Maloof JN, Straume M, Kay SA, Harmer SL. Global transcriptome analysis reveals circadian regulation of key pathways in plant growth and development. Genome Biol. 2008;9:R130.

54. Hughes ME, Hogenesch JB, Kornacker K. JTK_CYCLE: an efficient nonparametric algorithm for detecting rhythmic components in genome-scale data sets. J Biol Rhythms. 2010;25:372–80.

55. Hughes ME, Abruzzi KC, Allada R, Anafi R, Arpat AB, Asher G, et al. Guidelines for genome-scale analysis of biological rhythms. J Biol Rhythms. 2017;32:380–93.

56. Langfelder P, Horvath S. WGCNA: an R package for weighted correlation network analysis. BMC Bioinformatics. 2008;9:559.

57. Greenham K, Guadagno CR, Gehan MA, Mockler TC, Weinig C, Ewers BE, et al. Temporal network analysis identifies early physiological and transcriptomic indicators of mild drought in Brassica rapa. Elife. 2017;6:e29655.

58. Greenham K, Sartor RC, Zorich S, Lou P, Mockler TC, McClung CR. Expansion of the circadian transcriptome in Brassica rapa and genome-wide diversification of paralog expression patterns. Elife. 2020;9:e58993.

59. Dodd AN, Dalchau N, Gardner MJ, Baek S-J, Webb AAR. The circadian clock has transient plasticity of period and is required for timing of nocturnal processes in Arabidopsis. New Phytol. 2014;201:168–79.

60. Haydon MJ, Mielczarek O, Robertson FC, Hubbard KE, Webb AAR. Photosynthetic entrainment of the Arabidopsis thaliana circadian clock. Nature. 2013;502:689–92.

61. Hennessey TL, Field CB. Circadian rhythms in photosynthesis : Oscillations in carbon assimilation and stomatal conductance under constant conditions: Oscillations in carbon assimilation and stomatal conductance under constant conditions. Plant Physiol. 1991;96:831–6.

62. Wang S, Steed G, Webb AAR. Circadian entrainment in Arabidopsis. Plant Physiol. 2022;190:981–93.

63. Nagel DH, Doherty CJ, Pruneda-Paz JL, Schmitz RJ, Ecker JR, Kay SA. Genome-wide identification of CCA1 targets uncovers an expanded clock network in Arabidopsis. Proc Natl Acad Sci U S A. 2015;112:E4802–10.

64. Liu TL, Newton L, Liu M-J, Shiu S-H, Farré EM. A G-box-like motif is necessary for transcriptional regulation by circadian pseudo-response REGULATORs in Arabidopsis. Plant Physiol. 2016;170:528–39.

65. Sauret-Güeto S, Calder G, Harberd NP. Transient gibberellin application promotes Arabidopsis thaliana hypocotyl cell elongation without maintaining transverse orientation of microtubules on the outer tangential wall of epidermal cells: Gibberellins and microtubule orientation. Plant J. 2012;69:628–39.

66. Goh C-H, Lee DJ, Bae H-J. Gibberellic acid of Arabidopsis regulates the abscisic acid-induced inhibition of stomatal opening in response to light. Plant Sci. 2009;176:136–42.

67. Bordage S, Sullivan S, Laird J, Millar AJ, Nimmo HG. Organ specificity in the plant circadian system is explained by different light inputs to the shoot and root clocks. New Phytol. 2016;212:136–49.

68. Nimmo HG. Entrainment of Arabidopsis roots to the light:dark cycle by light piping. Plant Cell Environ. 2018;41:1742–8.

69. Wang Y, Huan Q, Li K, Qian W. Single-cell transcriptome atlas of the leaf and root of rice seedlings. J Genet Genomics. 2021;48:881–98.

70. Xia K, Sun H-X, Li J, Li J, Zhao Y, Chen L, et al. The single-cell stereo-seq reveals region-specific cell subtypes and transcriptome profiling in Arabidopsis leaves. Dev Cell. 2022;57:1299–310.e4.

71. Edwards KD, Anderson PE, Hall A, Salathia NS, Locke JCW, Lynn JR, et al. FLOWERING LOCUS C mediates natural variation in the high-temperature response of the Arabidopsis circadian clock. Plant Cell. 2006;18:639–50.

72. Hsu PY, Harmer SL. Wheels within wheels: the plant circadian system. Trends Plant Sci. 2014;19:240–9.

73. Schaffer R, Landgraf J, Accerbi M, Simon V, Larson M, Wisman E. Microarray analysis of diurnal and circadian-regulated genes in Arabidopsis. Plant Cell. 2001;13:113.

74. Matsushika A, Makino S, Kojima M, Mizuno T. Circadian waves of expression of the APRR1/TOC1 family of pseudo-response regulators in Arabidopsis thaliana: insight into the plant circadian clock. Plant Cell Physiol. 2000;41:1002–12.

75. Xue X, Sun K, Zhu Z. CIRCADIAN CLOCK ASSOCIATED 1 gates morning phased auxin response in Arabidopsis thaliana. Biochem Biophys Res Commun. 2020;527:935–40.

76. Covington MF, Harmer SL. The circadian clock regulates auxin signaling and responses in Arabidopsis. PLoS Biol. 2007;5:e222.

77. Hubbard KE, Webb AAR. Circadian rhythms in stomata: Physiological and molecular aspects. Rhythms in Plants. Cham: Springer International Publishing; 2015. p. 231–55.

78. Melotto M, Underwood W, Koczan J, Nomura K, He SY. Plant stomata function in innate immunity against bacterial invasion. Cell. 2006;126:969–80.

79. Zheng X-Y, Zhou M, Yoo H, Pruneda-Paz JL, Spivey NW, Kay SA, et al. Spatial and temporal regulation of biosynthesis of the plant immune signal salicylic acid. Proc Natl Acad Sci U S A. 2015;112:9166–73.

80. Goodspeed D, Chehab EW, Min-Venditti A, Braam J, Covington MF. Arabidopsis synchronizes jasmonate-mediated defense with insect circadian behavior. Proc Natl Acad Sci U S A. 2012;109:4674–7.

81. Booij-James IS, Swegle WM, Edelman M, Mattoo AK. Phosphorylation of the D1 photosystem II reaction center protein is controlled by an endogenous circadian rhythm. Plant Physiol. 2002;130:2069–75.

82. Dodd AN, Kusakina J, Hall A, Gould PD, Hanaoka M. The circadian regulation of photosynthesis. Photosynth Res. 2014;119:181–90.

83. Edelman M, Mattoo AK. D1-protein dynamics in photosystem II: the lingering enigma. Photosynth Res. 2008;98:609–20.

84. Cano-Ramirez DL, Panter PE, Takemura T, de Fraine TS, de Barros Dantas LL, Dekeya R, et al. Low-temperature and circadian signals are integrated by the sigma factor SIG5. Nat Plants. 2023;9:661–72.

85. Noordally ZB, Ishii K, Atkins KA, Wetherill SJ, Kusakina J, Walton EJ, et al. Circadian control of chloroplast transcription by a nuclear-encoded timing signal. Science. 2013;339:1316–9.

86. Jouve L, Gaspar T, Kevers C, Greppin H, Degli Agosti R. Involvement of indole-3-acetic acid in the circadian growth of the first internode of Arabidopsis. Planta. 1999;209:136–42.

87. Germain P-L, Lun A, Garcia Meixide C, Macnair W, Robinson MD. Doublet identification in single-cell sequencing data using scDblFinder. F1000Res. 2021;10:979.

88. Wu G, Anafi RC, Hughes ME, Kornacker K, Hogenesch JB. MetaCycle: an integrated R package to evaluate periodicity in large scale data. Bioinformatics. 2016;32:3351–3.

89. Conway JR, Lex A, Gehlenborg N. UpSetR: an R package for the visualization of intersecting sets and their properties. Bioinformatics. 2017;33:2938–40.

90. Huynh-Thu VA, Irrthum A, Wehenkel L, Geurts P. Inferring regulatory networks from expression data using tree-based methods. PLoS One [Internet]. 2010;5. Available from: http://dx.doi.org/10.1371/journal.pone.0012776

91. Aibar S, González-Blas CB, Moerman T, Huynh-Thu VA, Imrichova H, Hulselmans G, et al. SCENIC: single-cell regulatory network inference and clustering. Nat Methods. 2017;14:1083–6.

92. Cao S, He Z, Chen R, Luo Y, Fu L-Y, Zhou X, et al. scPlant: A versatile framework for single-cell transcriptomic data analysis in plants. Plant Commun. 2023;4:100631.

93. Shannon P, Markiel A, Ozier O, Baliga NS, Wang JT, Ramage D, et al. Cytoscape: a software environment for integrated models of biomolecular interaction networks. Genome Res. 2003;13:2498–504.

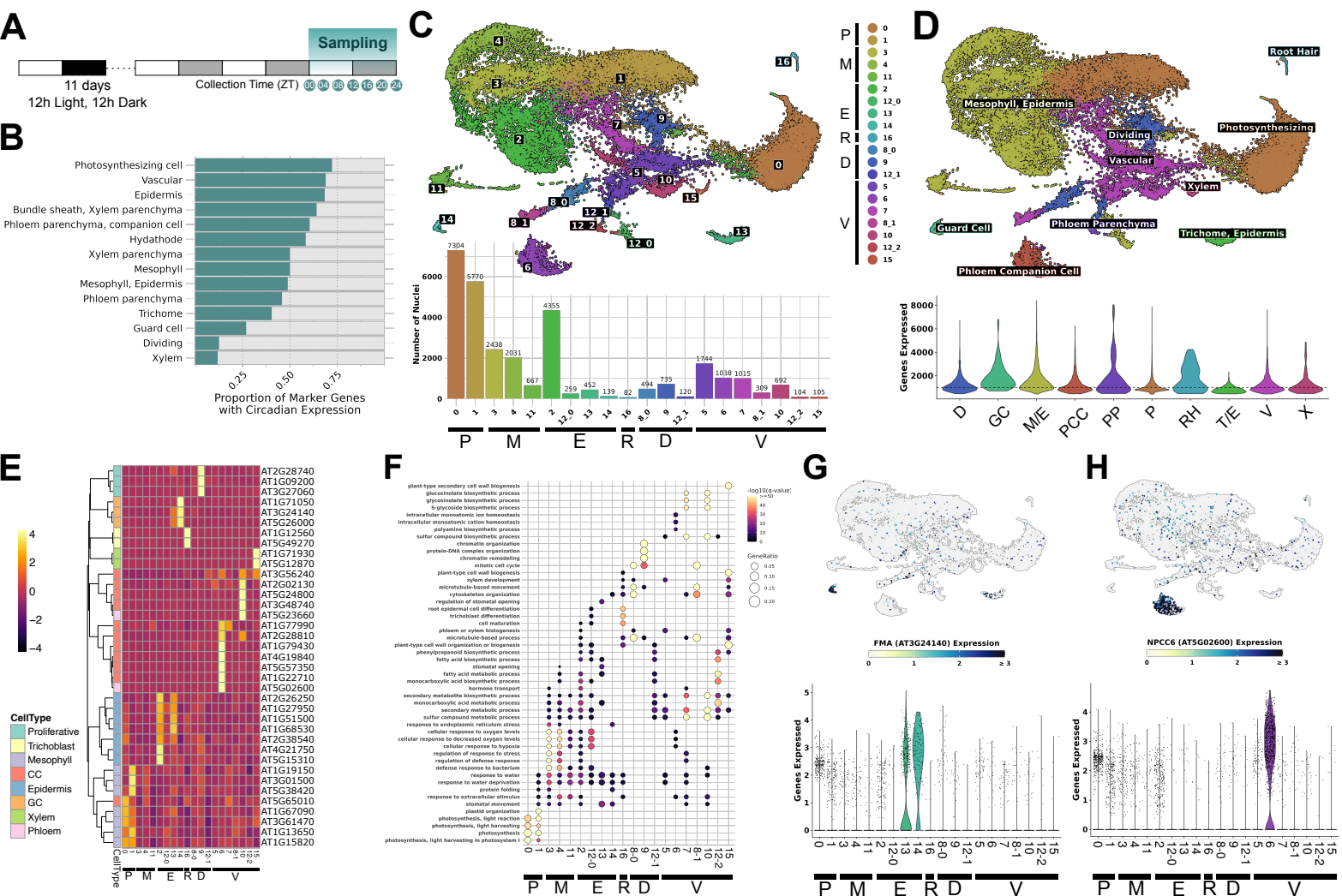
A
Sampling
11 days
12h Light, 12h Dark
Collection Time (ZT)
00 04 08 12 16 20 24
B
Photosynthesizing cell
Vascular
Epidermis
Bundle sheath, Xylem parenchyma
Phloem parenchyma, companion cell
Hydathode
Xylem parenchyma
Mesophyll
Mesophyll, Epidermis
Phloem parenchyma
Trichome
Guard cell
Dividing
Xylem
0.25
0.50
0.75
Proportion of Marker Genes with Circadian Expression
C
Number of Nuclei
P M E R D V
D
Root Hair
Mesophyll, Epidermis
Photosynthesizing
Dividing
Vascular
Xylem
Guard Cell
Phloem Parenchyma
Trichome, Epidermis
Phloem Companion Cell
Genes Expressed
D GC M/E PCC PP P RH T/E V X
E
CellType
Proliferative
Trichoblast
Mesophyll
CC
Epidermis
GC
Xylem
Phloem
F
-log10(q-value)
GeneRatio
G
FMA (AT3G24140) Expression
Genes Expressed
H
NPCC6 (AT5G02600) Expression
Genes Expressed

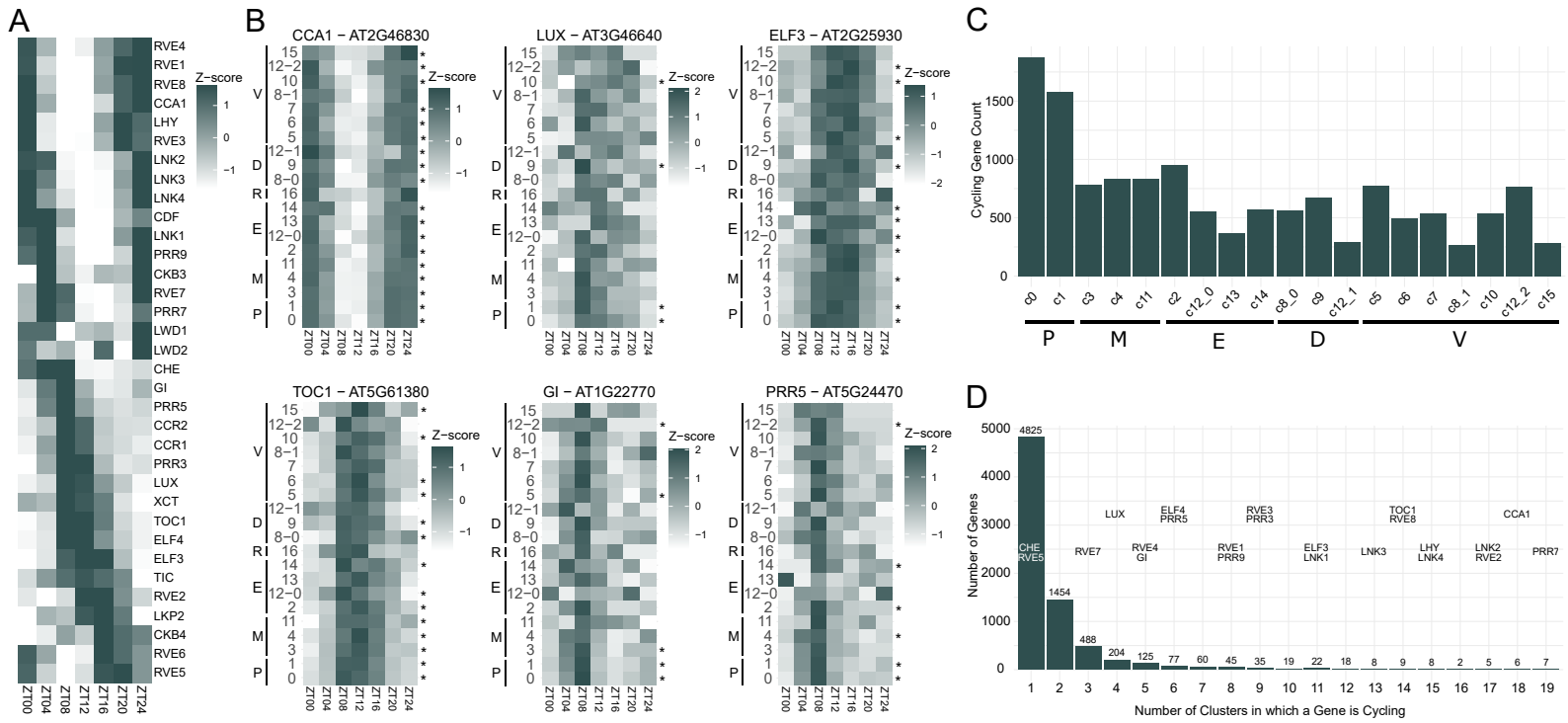
A
RVE4
RVE1
RVE8
CCA1
LHY
RVE3
LNK2
LNK3
LNK4
CDF
LNK1
PRR9
CKB3
RVE7
PRR7
LWD1
LWD2
CHE
GI
PRR5
CCR2
CCR1
PRR3
LUX
XCT
TOC1
ELF4
ELF3
TIC
RVE2
LKP2
CKB4
RVE6
RVE5
Z−score
ZT00 ZT04 ZT08 ZT12 ZT16 ZT20 ZT24
B
CCA1 − AT2G46830
LUX − AT3G46640
ELF3 − AT2G25930
TOC1 − AT5G61380
GI − AT1G22770
PRR5 − AT5G24470
V D R E M P
C
Cycling Gene Count
c0 c1 c3 c4 c11 c2 c12_0 c13 c14 c8_0 c9 c12_1 c5 c6 c7 c8_1 c10 c12_2 c15
P M E D V
D
Number of Genes
Number of Clusters in which a Gene is Cycling
4825 1454 488 204 125 77 60 45 35 19 22 18 8 9 8 2 5 6 7
CHE RVE5
RVE7
LUX
RVE4 GI
ELF4 PRR5
RVE1 PRR9
RVE3 PRR3
ELF3 LNK1
LNK3
TOC1 RVE8
LHY LNK4
LNK2 RVE2
CCA1
PRR7

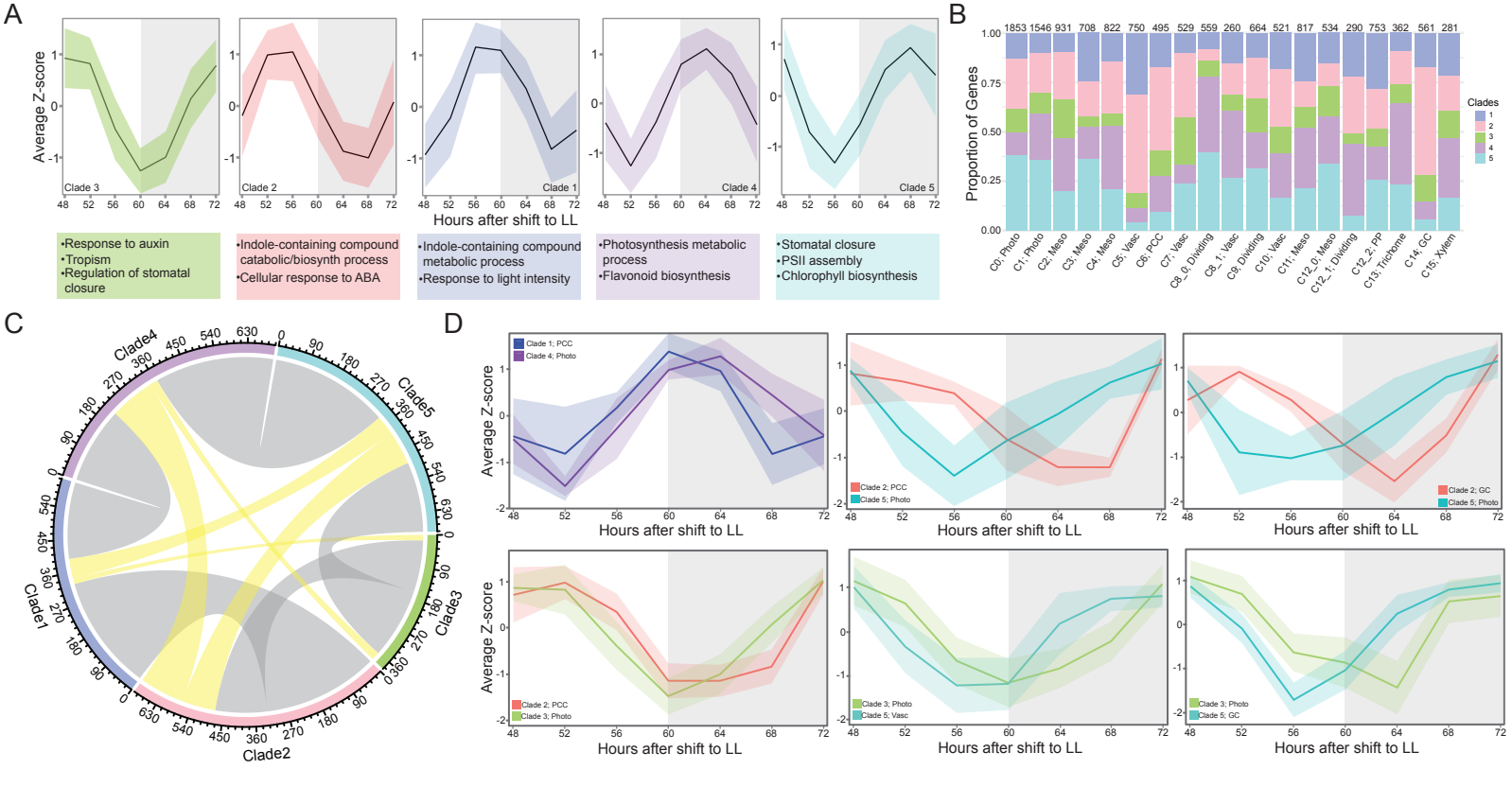
A
Average Z-score
Clade 3
Clade 2
Clade 1
Clade 4
Clade 5
Hours after shift to LL
•Response to auxin
•Tropism
•Regulation of stomatal closure
•Indole-containing compound catabolic/biosynth process
•Cellular response to ABA
•Indole-containing compound metabolic process
•Response to light intensity
•Photosynthesis metabolic process
•Flavonoid biosynthesis
•Stomatal closure
•PSII assembly
•Chlorophyll biosynthesis
B
1853 1546 931 708 822 750 495 529 559 260 664 521 817 534 290 753 362 561 281
Proportion of Genes
Clades
C0: Photo
C1; Photo
C2; Meso
C3; Meso
C4; Meso
C5; Vasc
C6; PCC
C7; Vasc
C8_0; Dividing
C8_1; Vasc
C9; Dividing
C10; Vasc
C11; Meso
C12_0; Meso
C12_1; Dividing
C12_2; PP
C13; Trichome
C14; GC
C15; Xylem
C
Clade1
Clade2
Clade3
Clade4
Clade5
D
Clade 1; PCC
Clade 4; Photo
Clade 2; PCC
Clade 5; Photo
Clade 2; GC
Clade 5; Photo
Clade 2; PCC
Clade 3; Photo
Clade 3; Photo
Clade 5; Vasc
Clade 3; Photo
Clade 5; GC
Average Z-score
Hours after shift to LL

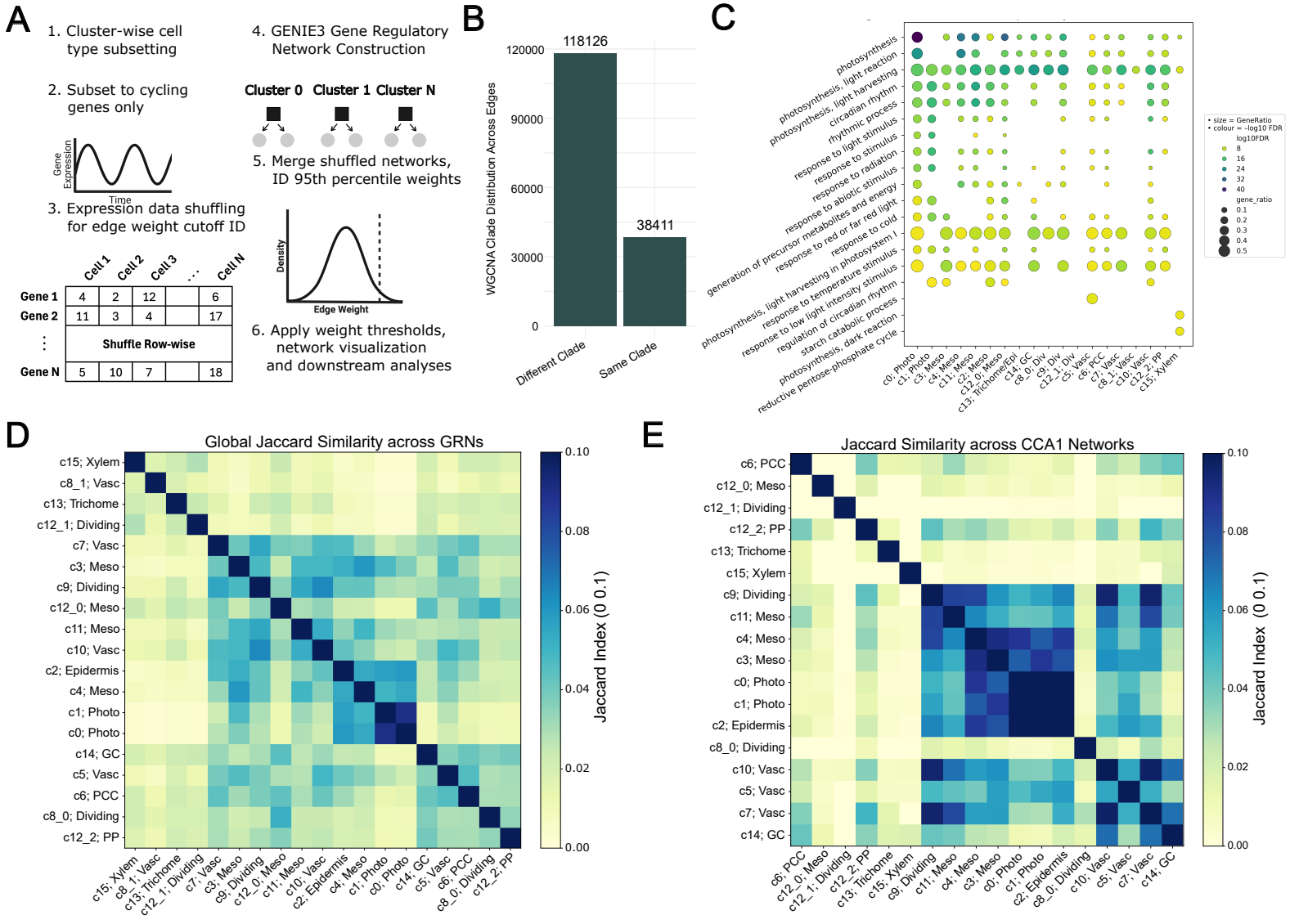
A
1. Cluster-wise cell type subsetting
2. Subset to cycling genes only
Gene Expression
Time
3. Expression data shuffling for edge weight cutoff ID
Cell 1
Cell 2
Cell 3
Cell N
Gene 1
Gene 2
Gene N
Shuffle Row-wise
4. GENIE3 Gene Regulatory Network Construction
Cluster 0
Cluster 1
Cluster N
5. Merge shuffled networks, ID 95th percentile weights
Density
Edge Weight
6. Apply weight thresholds, network visualization and downstream analyses
B
118126
38411
WGCNA Clade Distribution Across Edges
Different Clade
Same Clade
C
photosynthesis
photosynthesis, light reaction
photosynthesis, light harvesting
circadian rhythm
rhythmic process
response to light stimulus
response to stimulus
response to radiation
response to abiotic stimulus
generation of precursor metabolites and energy
response to red or far red light
response to cold
photosynthesis, light harvesting in photosystem I
response to temperature stimulus
response to low light intensity stimulus
regulation of circadian rhythm
starch catabolic process
photosynthesis, dark reaction
reductive pentose-phosphate cycle
size = GeneRatio
colour = -log10 FDR
log10FDR
gene_ratio
D
Global Jaccard Similarity across GRNs
Jaccard Index (0 0.1)
E
Jaccard Similarity across CCA1 Networks
Jaccard Index (0 0.1)

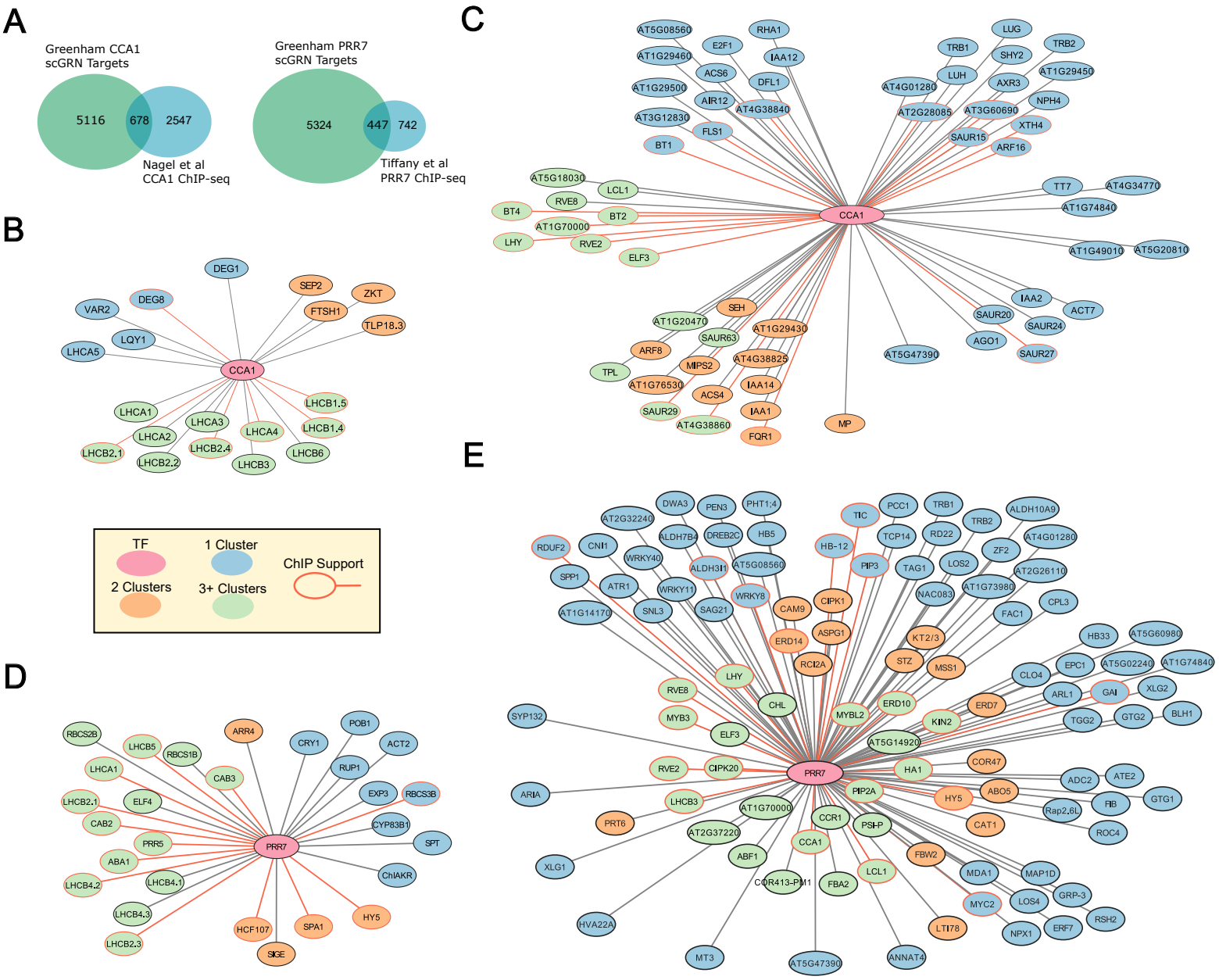
A
Greenham CCA1 scGRN Targets
5116
678
2547
Nagel et al CCA1 ChIP-seq
Greenham PRR7 scGRN Targets
5324
447
742
Tiffany et al PRR7 ChIP-seq
B
DEG1
SEP2
ZKT
VAR2
DEG8
FTSH1
TLP18.3
LQY1
LHCA5
CCA1
LHCB1.5
LHCA1
LHCA3
LHCA2
LHCA4
LHCB1.4
LHCB2.1
LHCB2.4
LHCB2.2
LHCB3
LHCB6
TF
1 Cluster
ChIP Support
2 Clusters
3+ Clusters
C
AT5G08560
RHA1
E2F1
AT1G29460
IAA12
ACS6
DFL1
AT1G29500
AIR12
AT4G38840
AT3G12830
FLS1
BT1
LUG
TRB1
TRB2
SHY2
LUH
AT1G29450
AT4G01280
AXR3
NPH4
AT2G28085
AT3G60690
XTH4
SAUR15
ARF16
AT5G18030
LCL1
RVE8
BT4
BT2
AT1G70000
LHY
RVE2
ELF3
CCA1
TT7
AT4G34770
AT1G74840
AT1G49010
AT5G20810
SEH
AT1G20470
AT1G29430
SAUR63
ARF8
MIPS2
AT4G38825
TPL
AT1G76530
IAA14
ACS4
SAUR29
IAA1
AT4G38860
FQR1
MP
AT5G47390
IAA2
ACT7
SAUR20
SAUR24
AGO1
SAUR27
D
RBCS2B
LHCB5
RBCS1B
ARR4
CRY1
POB1
ACT2
LHCA1
CAB3
RUP1
LHCB2.1
ELF4
EXP3
RBCS3B
CAB2
CYP83B1
PRR5
PRR7
SPT
ABA1
ChlAKR
LHCB4.2
LHCB4.1
LHCB4.3
HY5
HCF107
SPA1
LHCB2.3
SIGE
E
DWA3
PEN3
PHT1;4
AT2G32240
TIC
PCC1
TRB1
ALDH10A9
ALDH7B4
DREB2C
HB5
TRB2
RDUF2
CNI1
HB-12
TCP14
RD22
AT4G01280
WRKY40
ZF2
SPP1
ALDH3I1
AT5G08560
PIP3
TAG1
LOS2
AT2G26110
ATR1
WRKY11
WRKY8
NAC083
AT1G73980
AT1G14170
SNL3
SAG21
CAM9
CIPK1
CPL3
FAC1
ERD14
ASPG1
KT2/3
HB33
AT5G60980
RCI2A
STZ
MSS1
EPC1
AT5G02240
AT1G74840
LHY
CLO4
RVE8
CHL
ARL1
GAI
XLG2
MYBL2
ERD10
ERD7
SYP132
MYB3
KIN2
TGG2
GTG2
BLH1
ELF3
AT5G14920
RVE2
CIPK20
PRR7
HA1
COR47
ADC2
ATE2
ARIA
PIP2A
HY5
ABO5
FIB
GTG1
LHCB3
AT1G70000
Rap2.6L
PRT6
CCR1
PSI-P
CAT1
ROC4
AT2G37220
CCA1
ABF1
FBW2
XLG1
LCL1
MDA1
MAP1D
COR413-PM1
FBA2
MYC2
LOS4
GRP-3
HVA22A
LTI78
NPX1
ERF7
RSH2
MT3
AT5G47390
ANNAT4